JOURNAL OF APPLIED PHYSICS **108**, 114918 (2010)

Shock wave propagation in dense particle suspensions

Oren E. Petel[a] and Andrew J. Higgins
Department of Mechanical Engineering, McGill University, Montreal H3A 2K6, Canada

(Received 5 August 2010; accepted 22 September 2010; published online 15 December 2010)

Shock wave propagation in a multiphase suspension is studied experimentally. Particle suspensions are used as a means of obtaining a system in which there is limited initial interparticle contacts with a large degree of parametric variability. Suspensions were created in ethylene glycol at several volume fractions (41%, 48%, and 54%) of silicon carbide particles. Plate impact experiments are conducted to obtain the shock Hugoniots of the various suspensions at particle velocities in the range of 200–900 m/s. Transitions are shown to exist in the U_s-u_p Hugoniots of the suspensions. *In situ* longitudinal and lateral stress measurements are made in the 48% suspension at two different impact velocities demonstrating a deviatoric stress component to the stress state in the suspension. The results are discussed in terms of the development of extensive interparticle contacts in a mechanism analogous to classical shear thickening in dense suspensions. © *2010 American Institute of Physics*. [doi:10.1063/1.3504858]

I. INTRODUCTION

Recently, there has been considerable interest in shear thickening fluids for ballistic protection applications. Combinations of shear thickening fluids with traditional ballistic fabrics have been shown to enhance the ballistic protection offered by the fabrics alone.[1–3] However, the dynamic behavior of the shear thickening fluids themselves has yet to be thoroughly characterized under the stress levels associated with ballistic events. Split–Hopkinson pressure bar experiments have demonstrated that some shear thickening suspensions exhibit a sudden stiffening under uniaxial stress conditions,[4] however the stresses associated with these experiments are orders of magnitude lower than those seen in ballistic events. Alternatively, plate impact experiments can be used to elucidate the behavior of these fluids under the high strain rate, extreme stress environments associated with ballistic events.

Traditional shear thickening fluids are particle suspensions which exhibit non-Newtonian rheological properties when perturbed to a sufficient extent. The non-Newtonian behavior in these suspensions is a result of a relatively short timescale of perturbation in relation to the longer timescale of particle relaxation caused by the repulsive and hydrodynamic forces which maintain equilibrium within the suspension.[5–8] High particle volume fraction suspensions can exhibit drastic shear thickening, whereby a sufficient perturbation can lead to a discontinuous increase in viscosity within the suspension. This behavior is commonly discussed in terms of a clustering of particles forming flow blocking compacts within the suspension which behave similar to solids.[9,10] The development of these clusters can occur in both dilute and dense suspensions, albeit with differing degrees of magnitude.

Under shock wave loading, a phenomenon analogous to shear thickening may exist in which the greater compressibility of the liquid results in the development of significant interparticle contacts within the suspensions. In an impact, where a shock wave is transmitted into a suspension, the initial equilibrium state can be altered in such a way that promotes significant particle contacts. At the stress levels generated by intermediate velocity plate impacts, in the range of 100–1000 m/s, a solid phase can be chosen such that it is effectively incompressible, while the liquid will undergo large density variations due to its compressibility. As the density of the liquid phase increases under compression, the effective volume fraction of the suspension will increase, leading to the development of considerable interparticle contact networks.

Static compaction experiments on granular materials have demonstrated that stress transmission is accomplished through force chains of intergranular contacts.[11–15] These force chains are nonlinear and highly dependant on the relative orientation and shape of the grains in the system.[16,17] The statistical nature of these force chains often results in large forces being transmitted through a relatively small network of granular contacts or clusters, a phenomenon known as stress bridging. The randomized manner in which the forces are transmitted through the granular network leads to mesoscopic anisotropy in the granular media.[18,19] This has been demonstrated in extensive work using photoelastic techniques to visualize stress concentration in two-dimensional systems of circular grains.[20–22] Furthermore, this has been verified in dynamic mesoscale simulations which have demonstrated that the bulk shock response of granular media is dependent on the original granular orientation of the media.[23] The formation of these networks of force transmitting granular contacts can be shown to develop well before the random close packing limits of the granular system; therefore the clusters could maintain large pockets of the interstitial fluid within their structures. It is of interest to see if this picture developed from static environments translates into the shock compression domain.

At present, shock wave propagation in multiphase systems is often simulated with continuum level models. Con-

---

[a] Electronic mail: oren.petel@mail.mcgill.ca.

tinuum mixture models, which are less expensive computationally, are dependent on interphase exchange terms.[24–27] These exchange terms are primarily extensions of empirically determined coefficients used to close the system of governing equations in the model. Thus, the validation of these models requires data sets with well-documented variations in mixture length scales and loading fractions.

Mesoscale models, which focus on predicting bulk material response based on the interactions of mixtures on the individual component lengthscale, have been instrumental in clarifying some of the complex dynamic behavior exhibited by multiphase mixtures.[28–32] With the ever increasing computational power available to researchers, mesoscale modeling is an attractive computational approach. As in the case of continuum mixture models, the mesoscale models must be validated against extensive data sets to verify the legitimacy of the mesoscopic interaction models.

While a number of data sets for multiphase Hugoniots have been published,[33,34] much of that data has been obtained at a single volume fraction of loading for each mixture, without a systematic variation in parameters. Additionally, the vast majority of this data has been obtained at pressures well beyond the elastic limits of the solid phase materials involved. Data for multiphase mixtures in the lower pressure ranges, where the solid phase retains its elastic behavior or in the range of an elastic-plastic transition in the solid phase, is scarce.

An ideal multiphase system for the validation of mesoscale models are solid-liquid suspensions due to the parametric flexibility that they provide. This parametric flexibility can be used to probe the relationship between the development of force chains on shock wave propagation within a multiphase system. The data currently available for multiphase mixtures has been limited in their preparations to mainly packed bed systems of the solid phase components of a mixture, where extensive particle contacts are initially present by definition. There has been some work that has involved the use of either epoxy or paraffin as the interstitial components allowing for a greater variation in the volume fractions of the solid phases investigated.[35,36] Unfortunately, with those methods it is difficult to obtain a truly dispersed solid phase. Suspensions, however, can maintain a system of particles in an equilibrium state relatively devoid of particle contacts through electric double layer repulsion. A requirement for a stable suspension is that the particles must be within the length scale restriction of being colloid-sized or smaller.

In the present study, plate impact experiments were conducted to obtain the U_s-u_p Hugoniots of particle suspensions at several initial volume fractions. Based on the ample evidence of the effects of phase-transition on the trends of U_s-u_p Hugoniots, it can be expected that the stiffening of a suspension, analogous to shear thickening, would be visible in the Hugoniot as well. In addition to velocity measurements, *in situ* stress measurements were made within the suspensions in both the longitudinal (axial) and lateral directions.

A second approach adopted in the present study is the comparative directional stress measurement.[37–40] These measurements, which have been previously used to determine the deviatoric component of stress within solid materials, were used in the present study to investigate the dynamic behavior of suspensions. In a liquid, it can be expected that these two principal stress components will be equal to the hydrodynamic pressure in the liquid. Conversely, a solid can sustain a difference in principal stresses, the difference of which can be related to the maximum shear strength within the material. The development of extensive particle contacts and force chain networks within the suspension under impact loading would result in a nonhydrodynamic behavior of the suspensions, in the sense that a deviatoric stress component could be observed within the suspensions.

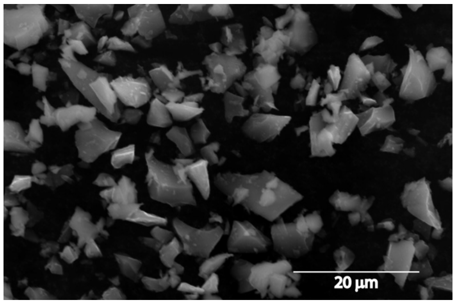

FIG. 1. SEM image of the silicon carbide powder.

II. EXPERIMENTAL DETAILS

The specific system of materials chosen for the present study was silicon carbide and ethylene glycol. This combination was chosen so that it was possible to produce a well-dispersed suspension of the solid phase in the liquid for the duration of the experiment. Previous studies have shown that similar mixtures can be maintained in a stable suspension for a sufficient period of time and that the suspension exhibits shear thickening behavior in certain ranges of solid volume fraction.[6,41] One major advantage of these solid-liquid suspensions is the possibility of varying the loading fraction of the solid phase while maintaining a near ideal dispersion. With this type of system, the volume fraction of the solid phase could be easily varied from the lower range of a 25% solid volume fraction, where the mixture is a translucent liquid, to upwards of 60% solid volume fraction, where the mixture has the texture of paste. By varying the volume fraction, the dominance of each phase can be examined and the influence of emerging force chains between the particles can be evaluated based on its effect on the wave propagation.

A. Mixture preparation

The silicon carbide, which was supplied by Washington Mills (Carborex-C5, 1200 grit, green α-SiC), was a mill-processed powder with an irregular morphology and a mean characteristic length scale of approximately 5–10 μm as seen in Fig. 1. The particle size distribution of these silicon carbide particles was obtained using a Malvern Mastersizer 2000 and is shown in Fig. 2. The ethylene glycol was supplied by ACP Chemicals with a 99.8% purity.

Silicon carbide was selected as the solid phase component for several reasons, the most important of which was favorable surface chemistry which enabled the particles to be

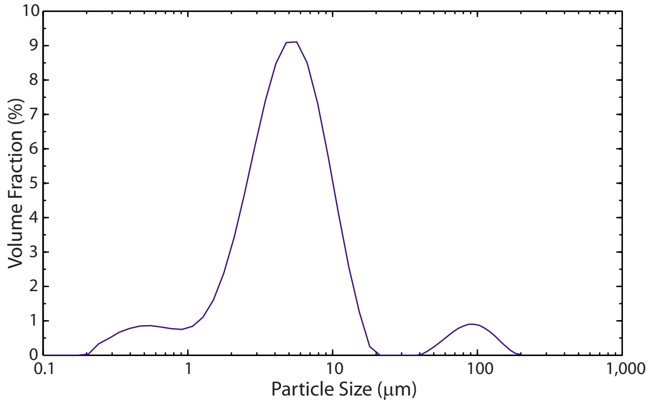

FIG. 2. (Color online) A particle size distribution for the silicon carbide particles. The $d(0.10)$, $d(0.50)$, and $d(0.90)$ particles sizes of the distribution are 1.514 μm, 4.664 μm, and 14.789 μm, respectively.

suspended in polar liquids (such as water or ethylene glycol).[41] Of the ceramic powders that could be suspended in this manner, silicon carbide was chosen for its large acoustic impedance and Hugoniot elastic limit. Ethylene glycol was chosen among polar fluids due to its low vapor pressure as well as the availability of shock Hugoniot data in the literature.[42] By studying a mixture of two components with such diverse material properties, the dominant physical role played by each component can be discussed in terms of shock propagation within the mixture.

The ethylene glycol was initially degassed under vacuum for a period of 15 min prior to being mixed with the silicon carbide. The components were prepared in a simple blender, adding solid to liquid until the appropriate mass fraction was achieved. The mixtures were then placed on a vortex mixer for a 24 h period at approximately 2000 rpm. Immediately prior to filling the experimental test cells, the mixtures were vacuum degassed while remaining on the vortex mixer for a period of 15 min to remove any trapped gasses that were not removed by the vortex mixer alone. The settling times for the suspensions were longer than 24 h and the experiments were conducted within an hour of the final degassing phase of the mixture preparation. During the test cell filling process, the mixtures were intentionally spread over the gages to ensure good coupling with the test gages prior to filling the entire test cell. The densities of the mixtures were measured either with a pycnometer or in the experimental test cell itself. The densities of the various mixtures were consistently within 1% of the expected theoretical density based on the mixing fractions. Three suspensions that were tested contained 41%, 48%, and 54% silicon carbide by volume.

B. Gas gun experiments

The planar impact experiments were performed with two different plate launching techniques: a gas gun and an explosively launched flyer plate. The helium driven single-stage gas gun had a barrel with a 64 mm internal bore. The sabot of the flyer plate was fitted with a magnet and the end of the barrel was lined with four induction gages, used to measure the velocity of the flyer plate as it exited the muzzle.

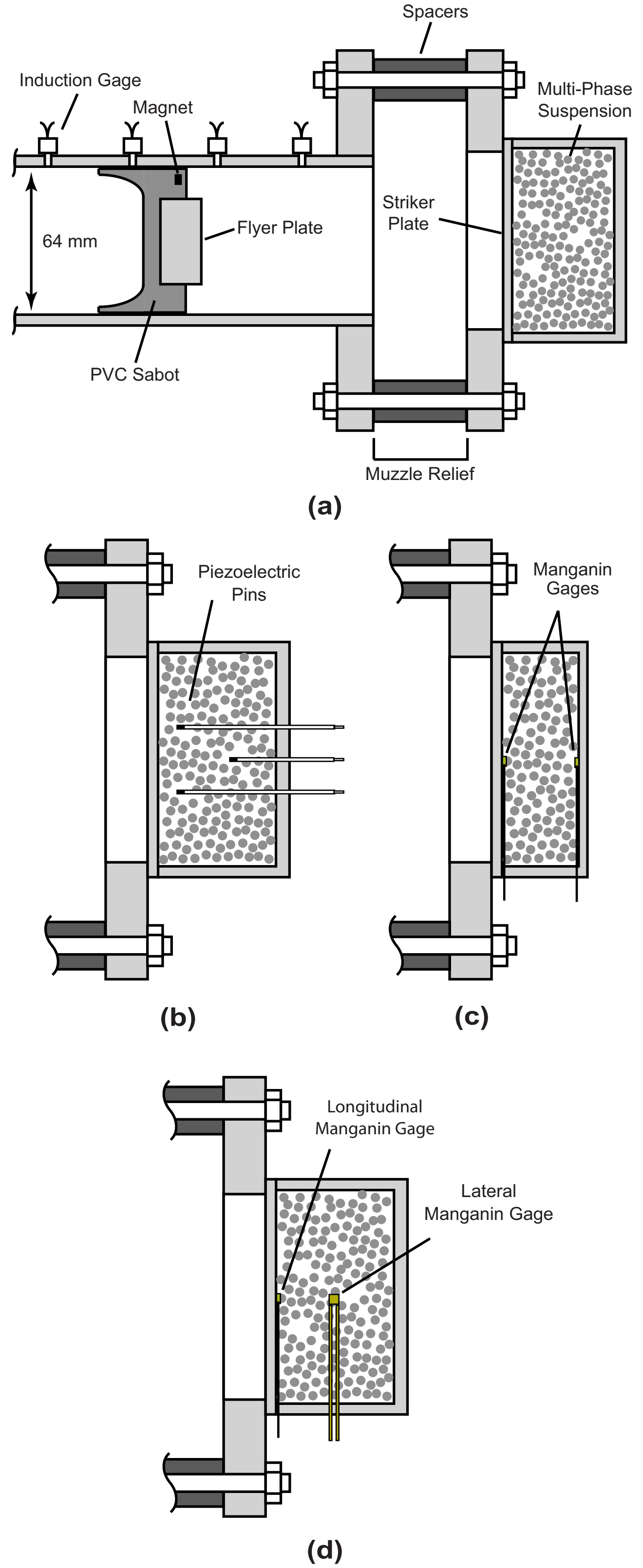

FIG. 3. (Color online) (a) Cross-sectional schematic of the muzzle of the single-stage gas gun and test cell. Expanded test cell schematic: (b) for velocity measurement using piezoelectric pins; (c) velocity and stress measurement involving manganin gages; and (d) directional stress measurements.

The experimental test cell was fixed at the muzzle of the gun with a constant standoff distance of 50 mm ensured by four precision steel spacers [Fig. 3(a)]. The spacers were used to provide muzzle relief, ensuring that a slug of air would not cushion the impact of the plate on the target. Furthermore, the sealed test cells were contained within a larger chamber which was evacuated along with the length of the barrel to below 5 kPa prior to each experiment, further reducing the influence of the precursor shock driven by the projectile.

Three types of experiments were conducted with the gas gun: shock wave velocity measurement with piezoelectric pins [Fig. 3(b)]; shock wave velocity measurements with manganin gages [Fig. 3(c)]; and directional stress measurement experiments [Fig. 3(d)]. Mild steel was used as the material for both the flyer and striker plates in order to ensure a symmetric impact. The striker plate had a diameter of 75 mm and a thickness of 3 mm.

1. Shock wave velocity measurements using piezoelectric pins

In these experiments the arrival time of the shock wave was monitored with piezoelectric pins (Dynasen, CA-1135) which were placed on a radius of 3 mm around the center of the test cell at distances of 5 and 15 mm from the bottom face of the striker plate. A cross-sectional schematic of the test cell is shown in Fig. 3(b). Four pins were used in each experiment, which allowed for the measurement of both the planarity and velocity of the incident shock wave. The averaged planarity of the shock wave was 25 mrad and 54 mrad at the first and second set of pins, respectively. The diameter and depth of the test cell were 50 mm and 25 mm, respectively.

The flyer plate used in these experiments had a diameter of 60 mm and a thickness of 3 mm. These experiments required wider flyer plates to limit the effects of lateral expansion and obtain accurate velocity data. The thickness of the flyer plate did not influence the results of the experiments as later manganin gage experiments using thicker flyer plates are in close agreement with the results of the piezoelectric pin measurements.

2. Shock wave velocity measurements using manganin gages

The test cell for this series of experiments contained two manganin piezoresistive stress gages (Vishay Micro-Measurements gage LM-SS-110FB-048/SP60) as illustrated in Fig. 3(c). The front manganin gage was fixed in the center of the rear surface of the striker plate, inside of the suspension, and the rear manganin gage was fixed in the center of the inner surface of the baseplate. The test cell depth was 5 mm and the flyer plate had a diameter of 38 mm and a thickness of 9 mm. The instrumentation of these experiments generated both shock wave velocity data as well as stress measurements within the mixtures.

3. Directional stress measurements using manganin gages

The test cell for this series of experiments also contained two manganin piezoresistive stress gages, however, their orientation differed slightly as illustrated in Fig. 3(d). The top manganin gage was fixed in the center of the rear surface of the striker plate and was used to measure the longitudinal stress component within the test cell. The lateral stress component was measured with a manganin gage which was fixed to a Mylar bridge that was strung across the test cell with the sensing element positioned perpendicular to the shock front. The center of the lateral gauge sensing element was positioned 5 mm from the longitudinal manganin gage position. The test cell depth was 25 mm and the flyer plate had a diameter of 38 mm and a thickness of 9 mm.

C. Explosively launched flyer plate experiments

In order to probe the response of the mixtures at higher impact velocities, an explosively launched flyer plate technique was used. These experiments were conducted in a mouse trap geometry, whereby the flyer plate was inclined at an angle in order to have a planar impact on the intended target as shown in Fig. 4(a). The initial angle of inclination for each experiment was determined through a combination of theoretical estimates and experimental verification. The theoretical estimates were based on a combination of the Gurney method[43] with the correction factors for the plate angle introduced in Hirsch *et al.*[44] Piezoelectric pins were used to measure the velocity and planarity of the flyer plates. The average planarity of the flyer plates was measured to be 5.7 mrad. The configurations of the gages for these experiments can be seen in Fig. 4.

The flyer and striker plates used in this series of experiments were aluminum 6061-T6. The flyer plate for these experiments had dimensions of 70 mm × 100 mm × 6.4 mm. As a measure to improve the planarity of the flyer plate, a line wave generator was used to initiate the bulk explosive charge, and a spall ring of four sacrificial aluminum plates surrounded the flyer plate. The spall ring was used to eliminate the influences of the lateral explosive expansion from adversely affecting the plate planarity. The spall ring layers were 15 mm wide on the lateral and rear boundary, while it was 38 mm on the boundary adjacent to the line wave generator. The test cell containing the suspensions measured 38 mm in diameter and 5 mm in depth.

Two types of experiments were conducted with this explosively launched flyer plate configuration. The first type of experiment involved manganin gage based shock wave velocity measurements within the suspensions [Fig. 4(b)], while the second type of experiment involved directional stress measurements in the suspensions [Fig. 4(c)].

For the experiments measuring the shock wave velocities of the suspensions, the top manganin gage was fixed in the center of the bottom face of the striker plate and the bottom gage was fixed in the center of the top face of the steel baseplate in the test cell. Since the test cell in these experiments was sufficiently thin as compared to its width, the top manganin gage often was able to capture the arrival of both the incident shock wave and the wave reflected from the steel baseplate. The analysis of this data will be explained in the subsequent section of the paper. A sample of the typical longitudinal manganin gage traces from one experiment is shown in Fig. 5 with the arrival times of the incident and reflected shock waves denoted.

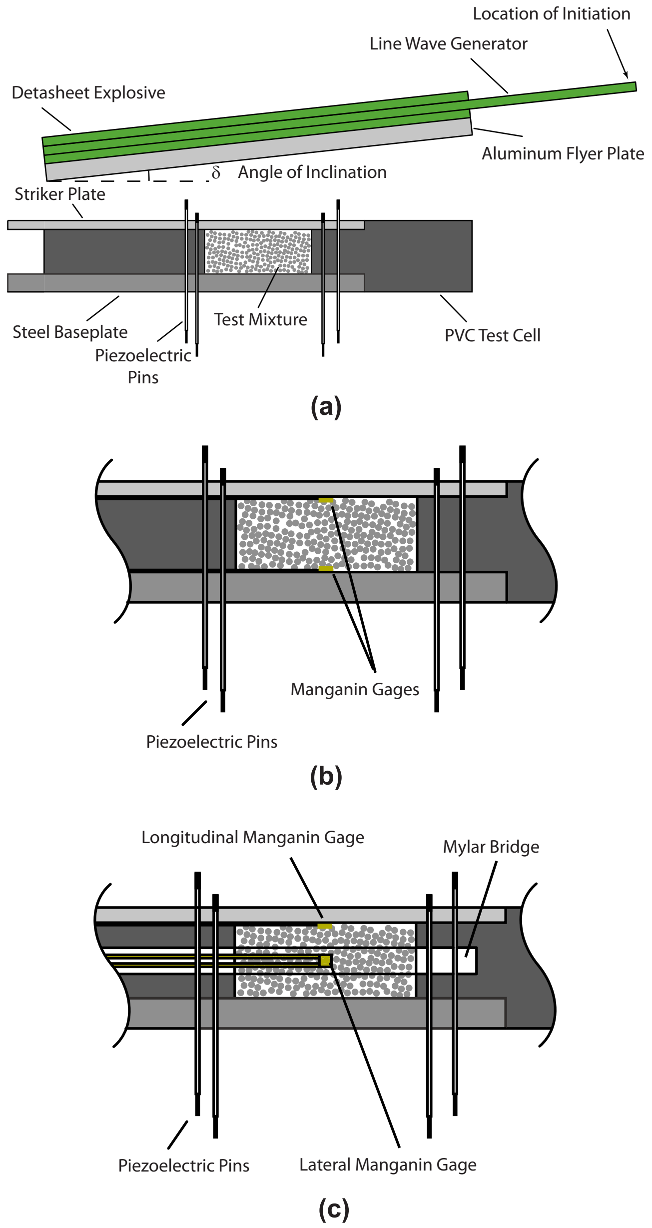

FIG. 4. (Color online) Cross-sectional schematics of (a) the explosively launched flyer plate experiments, (b) the test cell from velocity and stress measurement involving manganin gages, and (c) the test cell from directional stress measurements.

III. EXPERIMENTAL ANALYSIS

Although the results of the present study were derived from a combination of experimental configurations, some involving manganin gages and others involving piezoelectric pins, the experiments all measured the flyer plate velocity and the shock velocity in the test sample. In the absence of an *in situ* method of measuring the particle velocity of the mixture, it was necessary to calculate the particle velocity to locate the data on the U_s-u_p Hugoniot.

A. Incident shock wave analysis

The analysis of the wave interactions follows the impedance matching methods described at length by Cooper.[45] The impact of the flyer plate on the striker plate was designed to always result in a symmetric impact. Therefore, the conservation of mass and momentum across the left-going rarefaction fan in the striker plate, resulting from the shock interaction at the striker-mixture interface, can be combined to give the relationship

$$P_1 = \rho_0 C_0 (u_f - u_1) + \rho_0 S (u_f - u_1)^2, \tag{1}$$

where u_f is the measured flyer plate velocity, ρ_0 is the initial density of the flyer plate material, and C_0 and S are the coefficients of the linear fit to the Hugoniot data of the flyer plate material,[33] and P_1 and u_1 are the equilibrium pressure and particle velocity at the interface after the interaction, respectively.

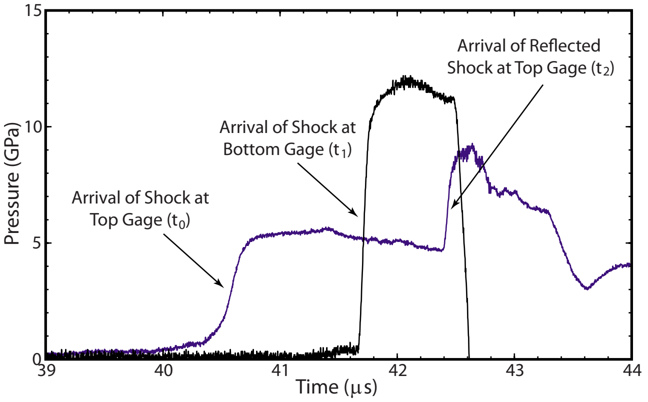

FIG. 5. (Color online) A sample set of manganin gage traces from an explosively launched flyer plate experiment designed for shock wave velocity measurements [Fig. 4(b)].

The equations of conservation of mass and momentum can similarly be combined for the shock wave entering the mixture due to this interaction,

$$P_1 = \rho_{0M} U u_1, \tag{2}$$

where ρ_{0M} is the mixture density and U is the measured shock wave velocity in the mixture. Notice that Eq. (2) remains general and does not make any assumptions *a priori* pertaining to the material properties of the mixture. Knowing the measured values of the flyer and shock velocities, Eqs. (1) and (2) can be solved to obtain the post-shock wave particle velocity at the interface, and thus in the mixture. This analysis assumes that the mixture itself is in equilibrium between its phases. As the characteristic length of the silicon carbide is approximately 5 μm, this assumption should hold. It should also be noted that since the striker plate was quite thin, 3 mm, the possibility of a two wave system in the mixture influencing the results was not a concern.

The conversion of the data from the U_s-u_p plane to the P-v plane was accomplished by solving the conservation of mass and momentum across the incident shock wave in the mixture for the post-shock pressure (P_1) and density (ρ_1)

$$\rho_{0M} U = \rho_1 (U - u_1), \tag{3}$$

$$P_1 - P_0 = \rho_{0M} U^2 - \rho_1 (U - u_1)^2. \tag{4}$$

B. Reflected shock wave analysis

In many of the explosive flyer plate experiments [Fig. 4(b)] it was possible to clearly see the signal from the re-

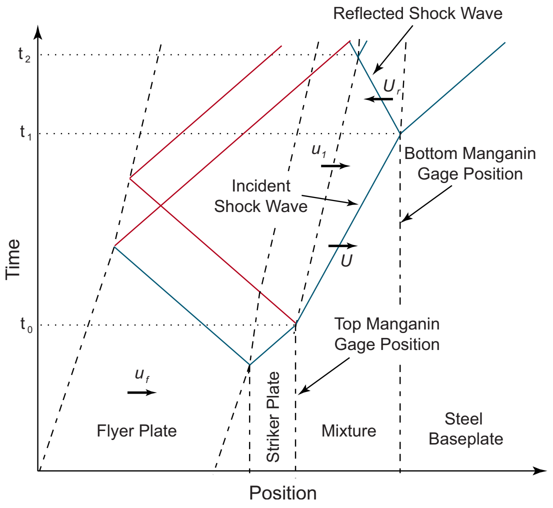

FIG. 6. (Color online) An x-t diagram of the incident and reflected wave relative to the manganin gages in the test cell.

flected shock wave on the top manganin gage. The mixture was confined between an aluminum striker plate and steel baseplate. Therefore, the incident wave in the mixture would reflect from the baseplate as a strong shock wave propagating back through the mixture. The location of the second shock wave arrival at the top manganin gage is clearly visible in Fig. 5. The paths of the incident and reflected waves within the test cell of these experiments can be tracked on a t-x diagram, as shown schematically in Fig. 6. The incident shock wave enters the mixture at time t_0, the incident shock wave reaches and reflects from the rear boundary at time t_1, and the reflected shock wave reaches the top manganin gage at time t_2.

The reflected wave in the mixture was analyzed with the following method. The speed of the wave was determined by the equation

$$U_r = \frac{x_2 - u_1(t_2 - t_0)}{t_2 - t_1}, \tag{5}$$

where U_r is the speed of the reflected wave, x_2 is the initial position of the bottom manganin gage relative to the top gage, u_1 is the particle velocity in the mixture resulting from the incident shock wave, and the times (t_0, t_1, and t_2) are defined in Fig. 6.

The equations of conservation of mass and momentum across the reflected shock wave can be written as

$$\rho_1(U_r + u_1) = \rho_2(U_r + u_2), \tag{6}$$

$$P_2 - P_1 = \rho_1(U_r + u_1)^2 - \rho_2(U_r + u_2)^2, \tag{7}$$

where P is the pressure, ρ is the density, u is the particle velocity, U_r is the reflected shock speed, and the subscripts 1 and 2 indicate the properties of the mixture behind the incident and reflected shock waves, respectively. The density of the mixture after being processed by the incident shock wave, ρ_1, can be determined from the continuity equation across the incident shock wave

$$\rho_1 = \rho_{0M}\frac{U}{(U - u_1)}. \tag{8}$$

The equation governing the properties behind the shock wave in the steel resulting from the wave reflection can be expressed as

$$P_2 = \rho_{0s}C_{0s}u_2 + \rho_{0s}S_s u_2^2, \tag{9}$$

where the subscript s indicates properties that are specific to the steel. Combining Eqs. (5)–(9), a solution can be found for the particle velocity behind the reflected shock wave, u_2. The pressure (P_2) and density (ρ_2) can then be found from Eqs. (6) and (7).

C. Mixture model

A simple mixture model was used to predict the Hugoniot of the various silicon carbide-EG suspensions for comparison to the collected data. This model was not used in the processing of the experimental data. The mixture model assumes that the state of mechanical equilibrium reached within the mixture can be determined by averaging the kinetic energy from their individual component Hugoniots on a mass basis in the P-u_p plane by the expression[46]

$$u_M^2 = \chi \cdot u_{\mathrm{SiC}}^2 + (1 - \chi) \cdot u_{\mathrm{EG}}^2, \tag{10}$$

where χ is the mass fraction of silicon carbide and the subscripts M, SiC, and EG represent the mixture, silicon carbide, and ethylene glycol, respectively. The particle velocities for the mixture components are taken from the individual Hugoniots of the components assuming pressure equilibrium between the phases. This mixture model was chosen as it is among the most accurate mixture models in the literature.[47] For this model, the silicon carbide was treated as an elastic solid, whose properties were taken from Munro,[48] and the ethylene glycol was modeled by a polynomial fit to its Hugoniot data presented in the subsequent section of this paper.

D. Directional stress measurements

A considerable body of research has been conducted on the use of manganin stress gages to measure the principal stresses within a material.[40,49–52] The calibration of the manganin gages in the present study followed the work of Rosenberg and Partom,[38,53] using the pressure dependent yield stress correction.[54] The maximum shear stress, within a solid body is related to the principal stresses through the relationship

$$\tau = \frac{\sigma_{\mathrm{Long}} - \sigma_{\mathrm{Lat}}}{2}, \tag{11}$$

where τ is the maximum shear stress, σ_{Long} and σ_{Lat} are the longitudinal and lateral stress components, respectively.

IV. EXPERIMENTAL SHOCK HUGONIOT RESULTS

A. Neat ethylene glycol

As validation of the experimental methods used in the present study, the shock Hugoniot of ethylene glycol measured. There is currently an existing set of shock Hugoniot

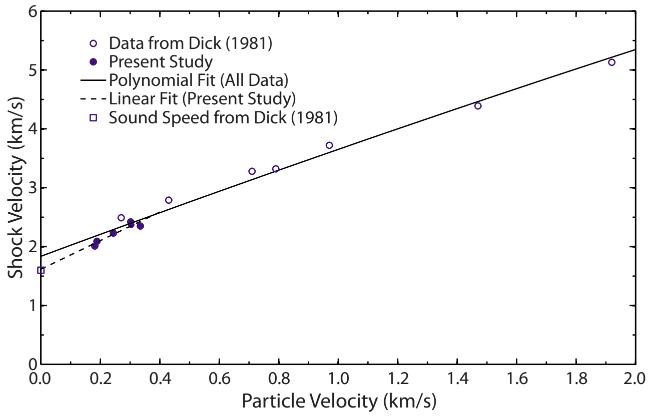

FIG. 7. (Color online) Comparison of Hugoniot data for ethylene glycol in the U_s-u_p plane.

data available in the literature for this liquid.[42] The results from the present study are compared to this existing data in the U_s-u_p plane in Fig. 7.

While the data from the present study resulted in slightly lower shock wave velocities than the previous data at similar particle velocities, a linear extrapolation of the present data back to the shock velocity axis illustrates that the sound speed of ethylene glycol is recovered accurately from the new data (Fig. 7). All of the data collected in the present study can be found tabulated in the Appendices.

With the addition of this new shock Hugoniot data for ethylene glycol, a polynomial expression encompassing the entire data set can be found using the form

$$U_s = C_0 + S_1 \cdot u_p + S_2 \cdot u_p^2, \tag{12}$$

where $C_0=1.84$ km/s, $S_1=1.88$, and $S_2=-0.061$ s/km are the fitting coefficients. This polynomial fit is shown relative to the data set in Fig. 7.

B. Results for the 41% silicon carbide volume fraction suspension

The suspension with the lowest density consisted of 41% silicon carbide (SiC) by volume fraction (66.8% by mass fraction) suspended in ethylene glycol and the suspension had an initial density of 1.98 g/cc. The results for this suspension from both the gas gun and explosive flyer experiments are shown in the U_s-u_p plane in Fig. 8 for the incident shock waves. The data is plotted in comparison to ethylene glycol as well as the mixture model of Eq. (10). Notice that in the low particle velocity range of the data, the Hugoniot data for the suspension is contained within the scatter of the neat ethylene glycol data. However, the two data sets diverge slightly in the higher particle velocity region. The mixture model has fair agreement within the range of collected Hugoniot data.

The data can also be examined in the P-v Hugoniot plane (Fig. 9). The U_s-u_p Hugoniot data was converted into this plane through Eqs. (3) and (4). In Fig. 9, both the incident and reflected shock wave data are presented along with the predictions of the mixture model. The reflected shock wave data seems to follow closely to the incident shock wave data as well as the mixture model predictions.

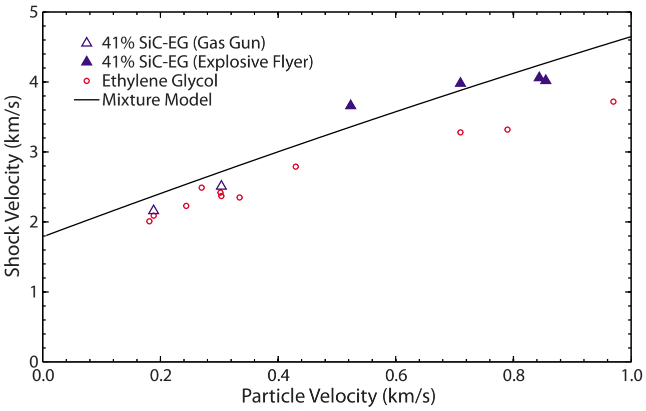

FIG. 8. (Color online) The experimental U_s-u_p Hugoniot data for the 41% silicon carbide volume fraction suspension.

C. Results for the 48% silicon carbide volume fraction suspension

The majority of the experiments in the present study were conducted with the intermediate solid loading of the 48% silicon carbide volume fraction (72.7% by mass fraction) suspension with an initial density of 2.12 g/cc. The results from the gas gun and explosive flyer plate are shown in the U_s-u_p plane in Fig. 10 for the incident shock wave in comparison to the mixture model prediction and the neat ethylene glycol data. Analyzing the data, it appears that there are two trends that exist in different particle velocity ranges for this mixture. In the lower range of particle velocity, the data of the mixture and ethylene glycol data are within experimental scatter, just as they were for the 41% mixture. However, at the higher range of particle velocities, the data diverges considerably from the neat ethylene glycol data. Consequently, the mixture model is unable to capture the shift in the Hugoniot data. The data seems to be more accurately represented by a series of linear fits as demonstrated in Fig. 11. The incident and reflected shock wave data is plotted in the P-v Hugoniot plane in Fig. 12 along with the linear trends introduced in Fig. 11.

Since most of the data collected in the lower range was obtained from the gas gun and all of the higher range data was collected with the explosive flyer technique, the upward shift in the experimental U_s-u_p data might be instinctively

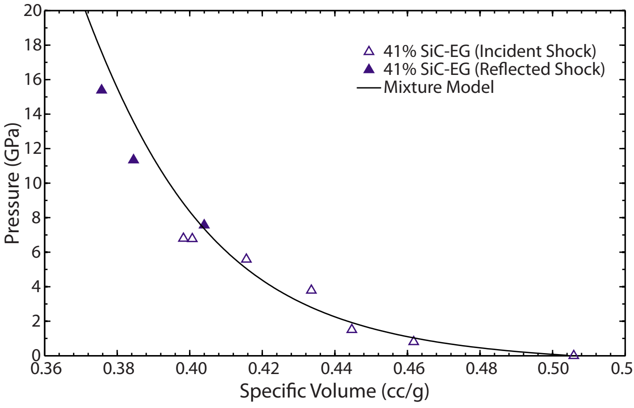

FIG. 9. (Color online) The experimental P-v Hugoniot data for the 41% silicon carbide volume fraction suspension.

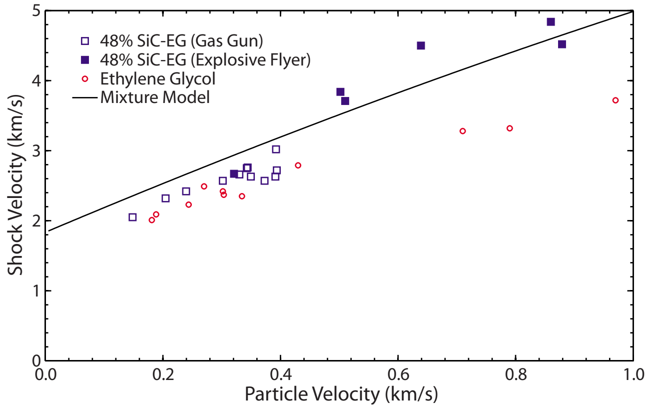

FIG. 10. (Color online) The experimental U_s-u_p Hugoniot data for the 48% silicon carbide volume fraction suspension.

attributed to the different techniques used. Note, however, that a data point obtained with the explosive flyer technique at a particle velocity of 0.32 km/s agrees well with the gas gun data, demonstrating an overlap in the results from the two techniques.

D. Results for the 54% silicon carbide volume fraction suspension

The highest density mixture in the present study consisted of a 54% volume fraction silicon carbide (77.3% by mass fraction) suspension with an initial density of 2.25 g/cc. It was not possible to make a mixture with a higher volume fraction while retaining the ability to fill a test cell reproducibly. Only a limited number of experiments were conducted with this mixture, the results of which are plotted in U_s-u_p plane in Fig. 13, along with the neat ethylene glycol data and the predictions of the mixture model. In contrast to the results from the lower concentration suspensions, the current mixture deviates from the ethylene glycol Hugoniot data beyond particle velocities of 200 m/s. The data from this suspension is also plotted in the P-v plane in Fig. 14. The agreement between the data and the model was excellent for this suspension.

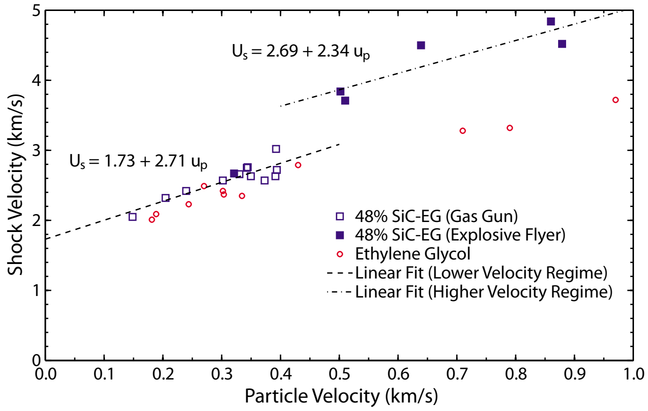

FIG. 11. (Color online) The experimental U_s-u_p Hugoniot data for the 48% silicon carbide volume fraction suspension with linear fits in different regions.

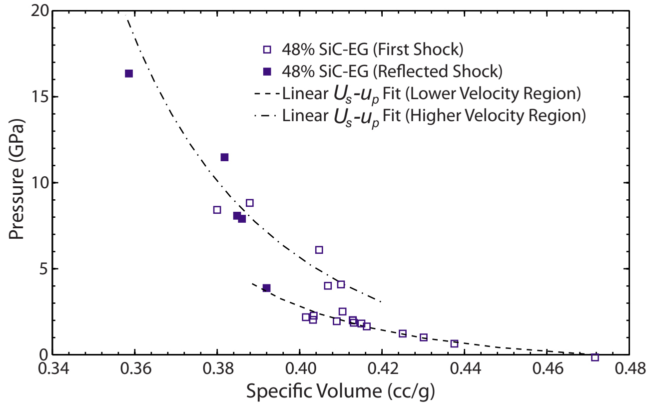

FIG. 12. (Color online) The experimental P-v Hugoniot data for the 48% silicon carbide volume fraction suspension.

V. DIRECTIONAL STRESS MEASUREMENTS

A. Neat ethylene glycol

As an effort to validate the experimental technique for liquids, measuring a hydrodynamic response with the manganin gages, two experiments were conducted using the explosive flyer plate configuration shown in Fig. 4(c) with neat ethylene glycol as the test material. A manganin gage was fixed to a 0.1 mm thick Mylar bridge, which was strung taut across the test cell with the sensing element perpendicular to the direction shock wave propagation in order to measure the lateral stress component in the test sample. A manganin gage was placed on the bottom face of the striker plate to measure the longitudinal stress component. While there is some limited data on the use of manganin gages to measure the longitudinal stresses in liquids,[37,55] there has yet to be a study that has successfully used lateral manganin gages in a liquid for validation purposes.

The two experiments involved an aluminum flyer plate with a velocity of 1050 ± 25 m/s. The stress histories for the two experiments are shown in Fig. 15. Unfortunately the longitudinal gage signals were cut prematurely by the shock wave, however, the two short plateaus in the signals are in close agreement with the peak stress measured by the lateral gages. The relatively long rise time (1 μs) of the lateral gage signals is consistent with the time required for the

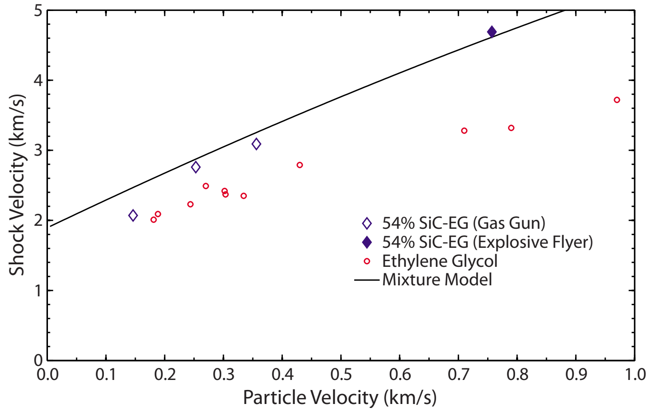

FIG. 13. (Color online) The experimental U_s-u_p Hugoniot data for the 54% silicon carbide volume fraction suspension.

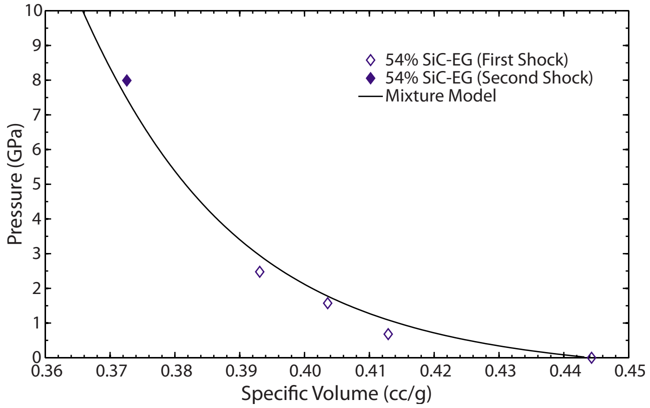

FIG. 14. (Color online) The experimental P-v Hugoniot data for the 54% silicon carbide volume fraction suspension.

shock wave to traverse the gage sensing element. The impact of the flyer plate at this velocity theoretically should have yielded a pressure of 3.2 GPa based the Hugoniot of ethylene glycol given by Eq. (12). A comparison to the manganin gage signals in Fig. 15 indicates that there is a 10% offset in the measured stresses. Alternatively, the quantitative agreement between the two measured principal stresses demonstrates that the two gage orientations recover the hydrodynamic response of the material, validating the technique with reproducibility.

B. 48% silicon carbide volume fraction suspension

Directional stress measurements were made in the 48% silicon carbide suspensions under two different impact loadings. The impact velocities of the flyer plates were chosen so that the measurements were taken on both sides of the apparent transition observed in the U_s-u_p Hugoniot of the suspension (Fig. 11).

1. Lower velocity region

Two experiments were conducted with the gas gun configuration [Fig. 3(d)] to probe the behavior of the mixture in the lower velocity region of the Hugoniot. The steel flyer plates used in these experiments had an impact velocity of 385 ± 20 m/s, which corresponds to a particle velocity in the mixture on the order of 340 m/s. The results of the experiments are shown in Fig. 16 with the lateral gage signals emphasized with thicker lines. Notice the agreement between each set of gages demonstrating reproducibility in the results.

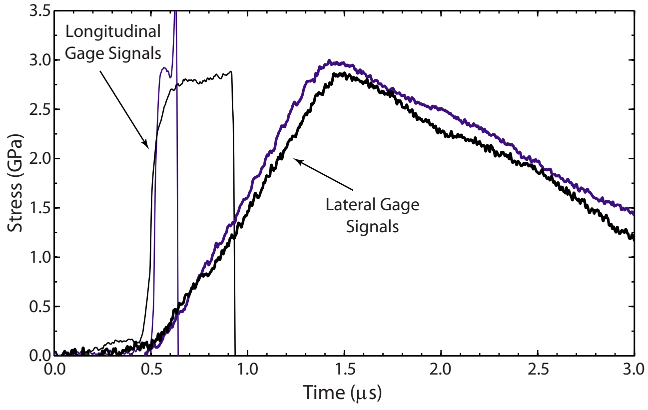

FIG. 15. (Color online) The stress histories of both longitudinally and laterally mounted manganin stress gages in neat ethylene glycol for an impact velocity of 1050 ± 25 m/s with an aluminum flyer plate.

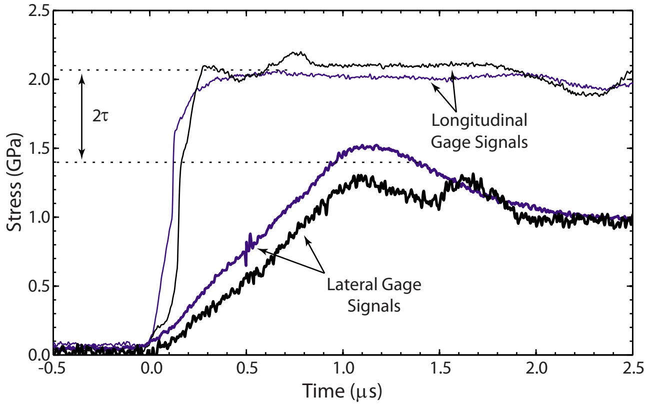

FIG. 16. (Color online) The stress histories of two sets of longitudinally and laterally mounted manganin stress gages in the 48% silicon carbide volume fraction suspension for an impact velocity of 385 ± 20 m/s with a steel flyer plate.

While it has been shown earlier that the Hugoniot of this suspension does not deviate significantly from the ethylene glycol Hugoniot at this loading condition, the state of stress within the mixture is qualitatively much different than that in neat ethylene glycol. The difference in the directional stresses within the suspension indicates that the suspension is able to maintain a shear stress, deviatoric component, much like an elastic solid would. The longitudinal stress within the suspension was approximately 2.05 ± 0.15 GPa, while the lateral stress component was approximately 1.40 ± 0.15 GPa. Therefore, the maximum shear stress within the suspension, based on Eq. (11), was approximately 0.30 ± 0.15 GPa.

2. Higher velocity region

Two experiments were conducted with the explosively launched flyer plate configuration [Fig. 4(c)] to probe the behavior of the mixture in the higher velocity region of the Hugoniot. The aluminum flyer plate had an impact velocity of 1050 ± 25 m/s, which corresponds to a particle velocity in the mixture on the order of 650 m/s. The results of these experiments are shown in Fig. 17, where the lateral gage signals are shown thicker than the longitudinal gage signals. Similar to the results for the lower velocity flyer plate, the behavior of the suspension in this region of the suspension Hugoniot is similarly not hydrodynamic. The suspension shows evidence of material strength, emphasized by the difference in the principal stresses within the suspension.

For this higher impact velocity experiment, the longitudinal stress within the suspension was approximately 5.4 ± 0.2 GPa, while the lateral stress component was approximately 4.4 ± 0.2 GPa. Therefore, the maximum shear stress within the suspension, based on Eq. (11), was approximately 0.5 ± 0.2 GPa.

An increase in the deviatoric stress component under increasing longitudinal stress was to be expected. For elastic solids, the deviatoric component increases with the longitu-

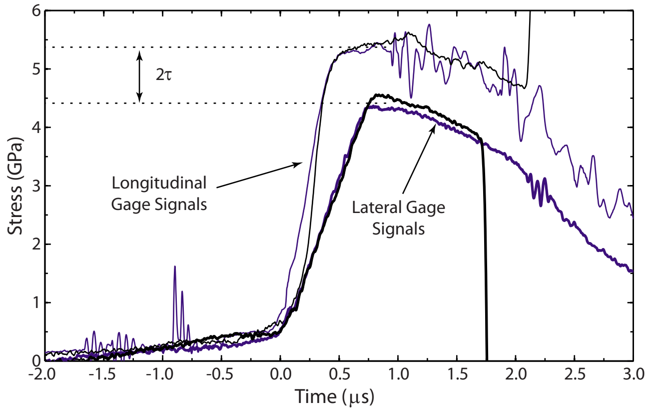

FIG. 17. (Color online) The stress histories of two sets of longitudinally and laterally mounted manganin stress gages in the 48% (volume fraction) silicon carbide-ethylene glycol suspension for an impact velocity of 1050 ± 25 m/s with an aluminum flyer plate.

dinal stress component until the Hugoniot elastic limit of the material is exceeded. While the same trend is seen with this suspension, it is not clear if the deviatoric stress component will continue to increase at even higher impact velocities or whether a limiting value will be reached as the solid component of the suspension will eventually undergo significant deformation.

VI. ANALYSIS AND DISCUSSION

At the lower range of particle velocities, the relation between shock velocity, and particle velocity (U_s-u_p) for the suspensions studied was nearly the same as that of neat ethylene glycol. This result, occurring in the near-acoustic regime, can be explained by considering the well-known relation for low-frequency acoustics in multiphase mixtures (the Wood's speed of sound)

$$\frac{1}{\rho_M C_M^2} = \frac{\chi_{\mathrm{SiC}}}{\rho_{\mathrm{SiC}} C_{\mathrm{SiC}}^2} + \frac{1-\chi_{\mathrm{SiC}}}{\rho_{\mathrm{EG}} C_{\mathrm{EG}}^2}, \tag{13}$$

where C is the sound speed of the specified component of the mixture and χ_{SiC} is the mass fraction of the silicon carbide. From Eq. (13), it is possible to obtain an estimate of the sound speed in the mixtures. Considering that the speeds of sound of silicon carbide and ethylene glycol are 11.82 km/s (Ref. 48) and 1.6 km/s (Ref. 42), respectively, the speed of sound for the 41%, 48%, and 54% silicon carbide volume fraction mixtures are 1.64 km/s, 1.74 km/s, and 1.85 km/s, respectively. This exercise demonstrates that in the low particle velocity range of the mixture Hugoniots, the dynamics of shock wave propagation are dominated by the compressibility of the ethylene glycol.

At the higher range of particle velocities studied, the suspensions exhibit behavior that is in agreement with the Hugoniot mixture model of Eq. (10), described in Sec. III C. In this regime, the suspensions exhibit a stiffer response in the U_s-u_p and P-v planes, indicating that the silicon carbide particles are in contact and strongly influence the wave propagation through the suspension.

All three suspensions exhibit a transition from a region of liquid-dominated wave propagation to a region suggestive of a phase-transition-like phenomenon as the particles begin to form extensive networks of contacts. This transition is most clearly evident in the 48% silicon carbide suspension, where there is an abrupt upward shift in the shock velocity response of about 1 km/s as the particle velocity exceeds 0.5 km/s.

Consider that the compressive strain behind a shock wave can be defined as

$$\varepsilon = \frac{u_p}{U_s}. \tag{14}$$

For a fixed value in particle velocity, a sharp increase in the shock velocity, as seen in the Hugoniot of the intermediate suspension (Fig. 11) corresponds to a decrease in the compressive strain in the mixture. Hence, the transition in the Hugoniot can be best described as a stiffening of the response of the suspension. Thus, the wave propagation in the mixture is no longer dominated by the compressibility of the liquid phase and is likely in a region of competing influences as suggested by the mixture model. Similar, although more pronounced, dilations in the strain of particles beds have been observed previously in plate impact experiments with dry nano-iron particles.[56,57]

It is of interest to calculate the volume fraction of the suspensions in the post-shock state. This can be accomplished by directly inserting experimentally measured properties into the mixture rules, assuming that the mass fraction of the suspension constituents is conserved across the shock front and that the silicon carbide is incompressible in these pressure ranges,

$$v_M = 1/\rho_M = \chi \cdot v_{\mathrm{SiC}} + (1-\chi) \cdot v_{\mathrm{EG}}, \tag{15}$$

$$\rho_M = \phi_{\mathrm{SiC}} \rho_{\mathrm{SiC}} + (1-\phi_{\mathrm{SiC}}) \rho_{\mathrm{EG}}, \tag{16}$$

where ϕ_{SiC} is the post-incident shock wave volume fraction of silicon carbide and all of the densities and specific volumes are the post-incident shock wave values. The results of this analysis are plotted for results from the different suspensions in Fig. 18.

When the data is plotted as shock pressure versus the volume fraction of silicon carbide, the transition to a stiffened behavior is clearly evident. Note, however, that the transition does not occur at one specific value of the post-shock volume fraction for the different suspensions. For the 48% initial loading, the transition occurs as the shock compression of the ethylene glycol results in the silicon carbide volume fraction reaching 55%. For the 41% initial loading, the transition appears to occur at around 46%–47%, and for 54% initial loading, the transition is less distinct, occurring around 57%. Thus, the transition does not appear to be a simple criterion of, for example, having the volume fraction exceed the random close packing limit of the suspended particles. The transition process appears to be a more complex process depending on the initial loading and the applied strain rate.

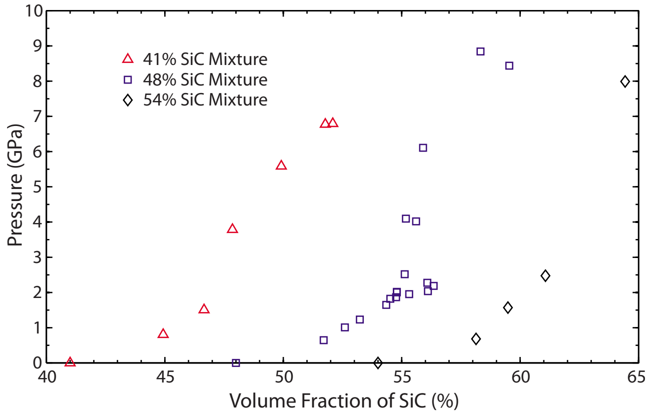

FIG. 18. (Color online) Comparison of the postincident shock wave volume fractions of silicon carbide for the three suspensions.

Measurements of deviatoric stress made with simultaneous longitudinal and lateral gages confirm that the transition is a complex process. While measurements in neat ethylene glycol confirm hydrodynamic conditions confirming no deviatoric stress), measurements made in the 48% initial volume fraction suspension at low particle velocities (where wave propagation is dominated by the liquid compressibility) do observe a deviatoric stress of approximately 0.3 GPa. This result implies that there is likely already some contact chain formation occurring prior to the distinct transition in the Hugoniot. While the state of stress within the suspension indicates influence from interparticle contacts, these contacts are not extensive enough to affect the wave propagation or the compressibility of the suspension as a whole. Deviatoric stress measurements made at an even greater particle velocity (above the sharp transition in the Hugoniot) find an even greater shear stress of 0.5 GPa, consistent with the idea that the suspension in this stress state is now increasingly dominated by the silicon carbide, in the form of extensive networks of interparticle contacts.

The anomalous behavior of the suspensions whereby the transition occurs at various volume fractions, with significant shear stress developing prior to the shift in the Hugoniot, could be attributed to several factors. The initial equilibrium distribution of the particles in suspension was random and thus upon shock compression the packing of the particles was far from ideal and will not evolve into a perfectly packed system, resulting in the behavior seen in Fig. 18. Additionally, the polydisperse size distribution and irregular particle morphology could contribute to the variation observed in the transition volume fraction. It can be expected that nonideal packing of particles with an irregular morphology results in the development of large pockets of interstitial fluids contained within granular structures. The transition in the Hugoniot is likely the result of the deformation of the suspension shifting from an ethylene glycol dominated deformation to a mixed region of deformation, whereby the newly formed contact network must be partly deformed in order to conserve the mass fraction of the mixture. It should be noted that the experimental analysis, outlined in Sec. III, remains valid even for a force chain-dominated wave propagation mechanism. The primary assumption of the analysis was that the system must reach mechanical equilibrium within the experimental timescale. This condition is satisfied experimentally as illustrated in Fig. 5, an experiment corresponding to a post-transition response, where the incident wave measured by the stress gauge has reached equilibrium promptly.

The development of a network of particle contacts should be expected to be highly strain rate dependent, given the disordered initial state of the suspension and the nature of shock compression. If the incident and secondary (reflected) shock wave Hugoniots of a material coincide, indicating loading path invariance, the material does not have a strong rate dependent response. A rate dependent response would involve a variation in the incident and reflected wave Hugoniots, as seen in the P-v plane in Fig. 12. Notice the trends representing the two linear U_s-u_p fits (from Fig. 11) and the relative location of the reflected shock wave data. There is one reflected data point which does not agree with the higher velocity fit, despite achieving a pressure in the range of behavioral transition for an incident shock wave. This reflected shock wave data point corresponds to an incident shock wave that was only slightly subcritical in terms of the Hugoniot transition (see Appendix, Tables IV and V, shot No. 17). Therefore, the mechanism that causes the transition in behavior appears to occur at a lower pressure for the incident shock wave as compared to the reflected shock wave, indicative of rate dependency in the transition.

VII. CONCLUSION

Extensive planar impact testing on suspensions of various volume fractions have demonstrated that even at low volume fractions, significant particle contacts and thus force chains can develop. These structural networks of clustered particles do not heavily influence the shock wave propagation velocity in the low particle velocity range, while they do influence the state of internal stress in the material, resulting in the existence of deviatoric stress components in the mixture.

At a given range of particle velocities, the Hugoniots of the mixtures transition to a behavior divergent from the liquid carrier component of the suspension. This transition seems to be indicative of a transition from a system where wave propagation is dominated by the compressibility of the liquid phase to either a mixed region of deformation or one where the wave propagation is fully supported by the system of particle contacts within the mixtures. The development and influence exhibited by these force chains on the wave propagation has been shown to be highly rate dependent through reflected shock wave experiments. The formation of these particle networks is speculated to be due to the relatively high compressibility of the liquid phase, raising the effective volume fraction of the silicon carbide particles, thus causing the particles to be driven into contact. This can best be described as a compression induced stiffening of the suspension, in analog to shear-induced thickening in conventional non-Newtonian fluids.

ACKNOWLEDGMENTS

The authors would like to thank David Frost for his support and suggestions in this effort and François Tang for his assistance in obtaining an SEM of the silicon carbide powder. The authors greatly appreciate the support and interest of Simon Ouellet of DRDC-Valcartier in this work. The assistance of Laurent Caudrelier and Surabhi Joshi in conducting the experimental work is much appreciated. The authors would also like to thank Nathalie Tufenkji and Petr Fiurasek for their enthusiastic assistance and generous access to their laboratory equipment. The authors appreciate the support of this work provided by the Natural Science and Engineering Research Council.

APPENDIX

The data that has been presented throughout the paper is tabulated in this appendix, organized by mixture. For data from the same mixture, coincident shot numbers in the incident and reflected shock wave tables correspond to results from a single experiment.

1. Neat ethylene glycol Hugoniot data

The incident shock wave Hugoniot data for neat ethylene glycol are shown in Table I.

2. 41% SiC-EG mixture Hugoniot data

Incident shock wave and reflected shock wave Hugoniot data for the 41% silicon carbide initial volume fraction suspension are shown in Tables II and III, respectively.

3. 48% SiC-EG mixture Hugoniot data

Incident shock wave and reflected shock wave Hugoniot data for the 48% silicon carbide initial volume fraction suspension are shown in Tables IV and V, respectively.

TABLE I. Incident shock wave Hugoniot data for neat ethylene glycol.

Shot No.	Flyer material	u_f (m/s)	u_p (m/s)	U_s (km/s)	P_{Measured} (GPa)
1	Steel	190	181	2.01	N/A
2	Steel	196	189	2.09	N/A
3	Steel	258	244	2.23	N/A
4	Steel	316	302	2.42	N/A
5	Steel	317	304	2.37	N/A
6	Steel	351	335	2.35	N/A

TABLE II. Incident shock wave Hugoniot data for the 41% silicon carbide initial volume fraction suspension.

Shot No.	Flyer material	u_f (m/s)	u_p (m/s)	U_s (km/s)	P_{Measured} (GPa)	SiC volume fraction (%)
1	Steel	206	188	2.16	N/A	44.9
2	Steel	336	304	2.51	N/A	46.6
3	Aluminum	1066	710	3.98	5.2	49.9
4	Aluminum	1280	855	4.02	6.4	52.1
5	Aluminum	1267	844	4.06	6.4	52.8
6	Aluminum	770	523.4	3.66	3.1	47.8

TABLE III. Reflected shock wave Hugoniot data for the 41% silicon carbide initial volume fraction suspension.

Shot No.	U_r (km/s)	ρ_2 (g/cc)	P_2 (GPa)	SiC volume fraction (%)
1	No reflected wave signal			
2	No reflected wave signal			
3	6.06	2.60	11.3	54.0
4	No reflected wave signal			
5	6.853	2.66	15.4	55.2
6	4.45	2.48	7.6	51.3

TABLE IV. Incident shock wave Hugoniot data for the 48% silicon carbide initial volume fraction suspension.

Shot No.	Flyer-striker material	u_f (m/s)	u_p (m/s)	U_s (km/s)	P_{Measured} (GPa)	SiC volume fraction (%)
1	Steel	443	394	2.72	N/A	56.0
2	Steel	338	302	2.57	N/A	54.2
3	Steel	163	148	2.05	N/A	51.6
4	PVC	559	240	2.42	N/A	53.1
5	PVC	474	205	2.32	N/A	52.5
6	Steel	417	373	2.57	N/A	56.0
7	Steel	386	343	2.75	N/A	54.7
8	Steel	447	392	3.02	N/A	55.0
9	Steel	392	350	2.63	2.25	55.2
10	Steel	370	330	2.66	1.8	54.7
11	Steel	388	344	2.76	2.1	54.7
12	Aluminum	1395	879	4.52	N/A	59.4
13	Aluminum	1400	860	4.84	8.2	58.2
14	Aluminum	772	502	3.84	N/A	55.1
15	Aluminum	1014	639	4.50	5.4	55.8
16	Aluminum	771	510	3.71	3.5	55.5
17	Aluminum	443	321	2.67	1.7	54.4

TABLE V. Reflected shock wave Hugoniot data for the 48% silicon carbide initial volume fraction suspension.

Shot No.	U_r (km/s)	ρ_2 (g/cc)	P_2 (GPa)	SiC volume fraction (%)
12	No reflected wave signal			
13	5.4	2.79	16.3	63.0
14	4.67	2.59	7.9	58.5
15	5.67	2.62	11.5	59.1
16	5.02	2.60	8.1	58.7
17	3.61	2.55	3.9	57.6

TABLE VI. Incident shock wave Hugoniot data for the 54% silicon carbide initial volume fraction suspension.

Shot No.	Flyer material	u_f (m/s)	u_p (m/s)	U_s (km/s)	P_{Measured} (GPa)	SiC volume fraction(%)
1	Steel	286	253	2.76	1.6	59.5
2	Steel	409	356	3.09	2.6	61.0
3	Steel	162	146	2.07	N/A	58.1
4	Aluminum	1250	757	4.69	N/A	64.4

4. 54% SiC-EG mixture Hugoniot data

Incident shock wave Hugoniot data for the 54% silicon carbide initial volume fraction suspension are shown in Table VI.

[1] Y. S. Lee, E. D. Wetzel, and N. J. Wagner, J. Mater. Sci. **38**, 2825 (2003).

[2] V. B. C. Tan, T. E. Tay, and W. K. Teo, Int. J. Solids Struct. **42**, 1561 (2005).

[3] E. D. Wetzel, Y. S. Lee, R. G. Egres, K. M. Kirkwood, J. E. Kirkwood, and N. J. Wagner, *Eighth International Conference on Numerical Methods in Industrial Forming Processes* (American Institute of Physics, Melville, NY, 2004), pp. 288–293.

[4] A. S. Lim, S. L. Lopatnikov, N. J. Wagner, and J. W. Gillespie, Jr., Rheol. Acta **49**(8), 879 (2010).

[5] H. A. Barnes, J. Rheol. **33**, 329 (1989).

[6] G. V. Franks, Z. Zhou, N. J. Duin, and D. V. Boger, J. Rheol. **44**, 759 (2000).

[7] J. Mewis and G. Biebaut, J. Rheol. **45**, 799 (2001).

[8] J. R. Melrose and R. C. Ball, J. Rheol. **48**, 937 (2004).

[9] R. S. Farr, J. R. Melrose, and R. C. Ball, Phys. Rev. E **55**, 7203 (1997).

[10] S. F. Edwards and D. V. Grinev, in *Jamming and Rheology: Constrained Dynamics on Microscopic and Macroscopic Scales*, edited by A. J. Liu and S. R. Nagel (Taylor & Francis, London, 2001), pp. 80–93.

[11] T. Travers, M. Ammi, D. Bideau, A. Gervois, J. C. Messager, and J. P. Troadec, Europhys. Lett. **4**, 329 (1987).

[12] T. Travers, M. Ammi, D. Bideau, A. Gervois, J. C. Messager, and J. P. Troadec, J. Phys. (Paris) **49**, 939 (1988).

[13] M. Ammi, T. Travers, D. Bideau, Y. Delugeard, J. C. Messager, J. P. Troadec, and A. Gervois, J. Phys.: Condens. Matter **2**, 9523 (1990).

[14] J. P. Troadec, D. Bideau, and J. A. Dodds, Powder Technol. **65**, 147 (1991).

[15] C.-H. Liu, S. R. Nagel, D. A. Schecter, S. N. Coppersmith, S. Majumdar, O. Narayan, and T. A. Witten, Science **269**, 513 (1995).

[16] M. Ammi, D. Bideau, and J. P. Troadec, J. Phys. D: Appl. Phys. **20**, 424 (1987).

[17] E. Azéma, F. Radjaï, R. Peyroux, and G. Saussine, *Traffic and Granular Flow '07* (Springer, Berlin, 2009), pp. 497–505.

[18] F. Radjai, M. Jean, J. J. Moreau, and S. Roux, Phys. Rev. Lett. **77**, 274 (1996).

[19] J.-P. Bouchaud, P. Claudin, D. Levine, and M. Otto, Eur. Phys. J. E **4**, 451 (2001).

[20] P. Dantu, in Proceedings of the Fourth International Conference on Soil Mechanics and Foundation Engineering, (Butterworth Scientific Publications, London, 1957), pp. 144–148.

[21] E. Guyon, S. Roux, A. Hansen, D. Bideau, J. P. Troadec, and H. Crapo, Rep. Prog. Phys. **53**, 373 (1990).

[22] J. Geng, G. Reydellet, E. Clément, and R. P. Behringer, Physica D **182**, 274 (2003).

[23] J. P. Borg and T. J. Vogler, Modell. Simul. Mater. Sci. Eng. **17**, 045003 (2009).

[24] M. R. Baer and J. W. Nunziato, Int. J. Multiphase Flow **12**, 861 (1986).

[25] J. M. Powers, D. S. Stewart, and H. Krier, ASME Trans. J. Appl. Mech. **56**, 15 (1989).

[26] J. B. Bdzil, R. Menikoff, S. F. Son, A. K. Kapila, and D. S. Stewart, Phys. Fluids **11**, 378 (1999).

[27] A. K. Kapila, R. Menikoff, J. B. Bdzil, S. F. Son, and D. S. Stewart, Phys. Fluids **13**, 3002 (2001).

[28] D. J. Benson, V. F. Nesterenko, F. Jonsdottir, and M. A. Meyers, J. Mech. Phys. Solids **45**, 1955 (1997).

[29] S. G. Bardenhagen and J. U. Brackbill, J. Appl. Phys. **83**, 5732 (1998).

[30] M. R. Baer, Thermochim. Acta **384**, 351 (2002).

[31] J. P. Borg, J. R. Cogar, A. Lloyd, A. Ward, D. Chapman, K. Tsembelis, and W. G. Proud, Int. J. Impact Eng. **33**, 109 (2006).

[32] J. P. Borg and T. J. Vogler, Int. J. Solids Struct. **45**, 1676 (2008).

[33] S. P. Marsh, *LASL Shock Hugoniot Data* (University of California Press, Los Angeles, 1980).

[34] A. V. Bushman, I. V. Lomonosov, and K. V. Khishchenko, "Shock wave data base," http://www.ficp.ac.ru/rusbank/, 2004.

[35] A. N. Dremin and I. A. Karpukhin, Zh. Eksp. Teor. Fiz. **1**, 184 (1960).

[36] D. E. Munson, R. R. Boade, and K. W. Schuler, J. Appl. Phys. **49**, 4797 (1978).

[37] Z. Rosenberg, D. Yaziv, and Y. Partom, J. Appl. Phys. **51**, 4790 (1980).

[38] Z. Rosenberg and Y. Partom, J. Appl. Phys. **58**, 3072 (1985).

[39] S. C. Gupta and Y. M. Gupta, J. Appl. Phys. **57**, 2464 (1985).

[40] J. C. F. Millett, N. K. Bourne, and Z. Rosenberg, J. Phys. D: Appl. Phys. **29**, 2466 (1996).

[41] R. Ramachandra Rao, H. N. Roopa, and T. S. Kannan, Ceram. Int. **25**, 223 (1999).

[42] R. D. Dick, J. Chem. Phys. **74**, 4053 (1981).

[43] R. W. Gurney, "The initial velocities of fragments from bombs, shells, and grenades," BRL Report 405, September 1943.

[44] E. Hirsch, P. C. Chou, and R. D. Ciccarelli, Propellants, Explos., Pyrotech. **11**, 53 (1986).

[45] P. Cooper, *Explosives Engineering* (Wiley-VCH, New York, NY, 1996).

[46] S. S. Batsanov, *Effects of Explosions on Materials: Modification and Synthesis under High-Pressure Shock Compression* (Springer-Verlag, New York, 1994), Vol. viii.

[47] O. E. Petel and F. X. Jette, Shock Waves **20**, 73 (2010).

[48] R. G. Munro, J. Phys. Chem. Ref. Data **26**, 1195 (1997).

[49] Z. Rosenberg, D. Yaziv, Y. Yeshurun, and S. J. Bless, J. Appl. Phys. **62**, 1120 (1987).

[50] Z. Rosenberg, N. S. Brar, and S. J. Bless, J. Appl. Phys. **70**, 167 (1991).

[51] J. C. F. Millett, N. K. Bourne, and Z. Rosenberg, J. Appl. Phys. **81**, 2579 (1997).

[52] J. C. F. Millett, N. K. Bourne, Z. Rosenberg, and J. E. Field, J. Appl. Phys. **86**, 6707 (1999).

[53] Z. Rosenberg, D. Yaziv, and Y. Partom, J. Appl. Phys. **51**, 3702 (1980).

[54] Z. Rosenberg and Y. Partom, J. Appl. Phys. **57**, 5084 (1985).

[55] A. J. Higgins, F. X. Jetté, A. Yoshinaka, and F. Zhang, in 12th Symposium (International) on Detonation, Office of Naval Research, San Diego, CA, 2002, pp. 993-1000.

[56] C. D. Dai, D. E. Eakins, N. N. Thadhani, and J. P. Liu, Appl. Phys. Lett. **90**, 071911 (2007).

[57] C. D. Dai, D. E. Eakins, and N. N. Thadhani, J. Appl. Phys. **103**, 093503 (2008).